Green Synthesis Of $Ag - Mg(OH)_2$ Nanocomposites Using Avocado Peel Extract And Study On Catalytic Properties In The Photodegradation Of Methylene Blue

Diep Tuong Minh Nhat[1], Nguyen Anh Duc[1], and Ngo Tran Hoang Duong[1,2*]

[1] *Faculty of Chemical Engineering, Ho Chi Minh City University of Technology (HCMUT), 268 Ly Thuong Kiet Street, Dien Hong Ward, Ho Chi Minh City, Vietnam*

[2] *Vietnam National University Ho Chi Minh City, Linh Xuan Ward, Ho Chi Minh City, Vietnam*

[*] *Corresponding author. E-mail: nthduong@hcmut.edu.vn*

Received: Aug. 29, 2025; Accepted: Dec. 10, 2025

The rapid development of Vietnam's textile dyeing industry has fueled economic growth, yet it has brought to light the issue of organic dye contamination in wastewater, posing environmental and public health concerns. In response, our work introduces an innovative approach to address this challenge: the synthesis of $Ag - Mg(OH)_2$ nanocomposites using avocado peel extract (*Perseaamericana*) for the efficient removal of organic dyes from wastewater. This novel method not only yields eco-friendly materials but also optimizes the use of agricultural by-products, aligning with principles of sustainability and green chemistry. By employing advanced analytical techniques, including Ultraviolet-Visible spectrophotometry (UV-Vis), X-ray diffraction (XRD), and scanning electron microscopy combined with energy-dispersive X-ray spectroscopy (SEM-EDX), the authors conducted a thorough characterization of the synthesized $Ag - Mg(OH)_2$ nanocomposites. The unique structural composition of the material was revealed, featuring silver nanoparticles (20 to 50 nm in diameter) evenly dispersed on $Mg(OH)_2$ nanorods (250 to 300 nm in length). In addition, the study explored the efficacy of these nanocomposites in the photocatalytic degradation of the cationic organic dye methylene blue (MB). A notably remarkable photodegradation efficiency was observed at 82.8% after 3 hours, with an initial aqueous MB concentration of 20 ppm and a material mass - liquid volume ratio of 8 g/L. The findings of this research are not only scientifically relevant, but also offer tangible solutions for mitigating environmental pollution and improving the quality of life.

Keywords: avocado peel extract, wastewater treatment, methylene blue, photodegradation, $Ag - Mg(OH)_2$ nanocomposites.

http://dx.doi.org/10.6180/jase.202611_34.013

1. Introduction

In the heart of Vietnam's growing textile industry, the demand to tackle environmental and health risks posed by organic dyes in wastewater emerges as a critical challenge. Regarding this issue, our scientific inquiry embarks on an ambitious sustainable solution, namely the synthesis and remedial use of the novel nanocomposite material $Ag - Mg(OH)_2$ [1–7]. The material is based on the dispersion of Ag nanoparticles synthesized via a plant extract-mediated reduction on an $Mg(OH)_2$ support produced via the *in situ* hydration of precursor MgO, which is generated from the sol-gel method. Such bottom-up phytosynthesis is considered less energy-consuming, more cost-effective and more eco-friendly than conventional physical and chemical routes, as well as the biosynthesis from algae and cyanobacteria species [8]. Technically, a broad range of native plants can be extracted for phytochemicals which help reduce metal ions and assemble nanoparticles. Menaa et al. have demonstrated that extracts from the leaves of *Tephrosia purpurea* (South Asia) and *Portulaca Oleracea* (North Africa) promote the formation of nano ZnO , an excellent photocatalyst to remove organic dyes Methylene Blue (MB) and Methyl Orange (MO) from wastewater [9, 10]. Inspired from these studies, our work utilizes the polyphenol-rich liquid extract of avocado peel (*Persea americana*), a common agricultural by-product mainly found in the Central Highlands of Vietnam, as the key factor to assist the production of $Ag-Mg(OH)_2$ nanocomposites [11, 12]. As avocado peel provides several bioactive compounds which function as reducing and capping agents to form Ag nanoparticles, it has been considered a potential candidate for the phytosynthesis process [13]. Compared to extracts from other polyphenol-rich herbs such as *Achillea* [14] and *Camellia sinensis* (green tea) [15], which are mostly applied in biomedicine fields, the avocado peel extract often yields a considerably higher phenolic content (beyond 310 mmol GA/100 g) [16]. Regarding the growing avocado production in Vietnam (approximately 200.000 tons per year), it is necessary to turn an abundant amount of avocado peel (biowaste) more beneficial through greener preparations of metal/metal oxide nanoparticles for extensive applications in drug delivery, food preservation and water remediation [17]. Meanwhile, the choice of $Ag-Mg(OH)_2$ nanocomposites in this study, rather than other permutations of metal nanoparticles - metal oxide/hydroxide support, closely relies on their specific physicochemical characteristics. Here, Ag nanoparticles, whose antibacterial [18] and catalytic properties [19] have been well established, are projected to be finely dispersed on $Mg(OH)_2$, a versatile carrier with excellent stability and environmental compatibility. It is noteworthy that MgO nanoparticles - the anhydrous form of $Mg(OH)_2$ - have been recently biosynthesized, exhibiting remarkable disinfection and photocatalytic activities, and even combined with Ag nanoparticles for synergistic antibacterial effects [20]. Jayapriya et al. have observed that green Ag/MgO nanocomposites work for the catalytic treatment of anthropogenic pollutants, as well as demonstrating anti-cancer and antimicrobial activities [7]. Meanwhile, Zidane et al. successfully synthesized AgO/Ag_2O and $MgO@AgO/Ag_2O$ nanocomposites using *Portulaca oleracea* leaf extract and recorded a well-improved photocatalytic activity from the 2-hour sunlight irradiation of MB (68% and 77% of degradation respectively) [21]. $Mg(OH)_2$ nanoparticles, however, under certain circumstances may offer a better option for metal deposition. Despite commonly lower catalytic and antimicrobial activities with respect to MgO , the hydroxide is more stable in aqueous solutions and more tolerant to moisture, which are standards for long-term preservation. Li et al. have found that $Mg(OH)_2$ nanoparticles even outperform MgO counterparts in terms of removing arsenate contaminants from wastewater, where the former eliminates most As(V) species in minutes while the latter fails [22]. Besides, Fang et al.'s work on reusable $CdS@Mg(OH)_2$ nanocomposites highlights that the $Mg(OH)_2$ layer strongly improves the stability and photocatalytic activity of CdS sites on water-splitting [23]. In fact, $Mg(OH)_2$ nanoparticles have gradually gained scientific interests through their strong antibacterial, antioxidant and anti-inflammatory potentials as reflected from Menaa et al.'s recent study, where the material was phytosynthesized using *Tinospora cordifolia* leaf extract [24]. These analyses render the combination of Ag and $Mg(OH)_2$ nanoparticles reasonable to essentially combat microbial contamination and offer a diverse array of environmental applications. In our work, the crystalline structure and surface morphology of $Ag-Mg(OH)_2$ nanocomposites can be determined through characterization techniques such as X-ray diffraction (XRD) and scanning electron microscopy (SEM). Such techniques provide valuable insights into mechanisms through which particles are formed and how the structure can be optimized to adapt for various purposes, including microbiological assays against various strains of bacteria [25] and water purification systems [26, 27]. Regarding these applications, our work is technically in line with studies using different oxide/hydroxide supports. For instance, Saoud et al. have discovered that highly stable Ag/WO_3 nanocomposites exhibit significant catalytic activity toward the degradation of MB under visible light [28]. Hasen et al. have observed the exceptional photocatalytic activity of *Laurus nobilis* leaf extract-derived $Ag@Fe_3O_4$ nanocomposites to decompose MB , Toluidine Blue (TB), and Rose Bengal in oily wastewater, along with promising antibacterial properties and biocompatibility [29]. Evidently, based on the antibacterial nature of Ag nanoparticles and its possibly enhanced photocatalytic activity when deposited on metal oxide/hydroxide supports [30], the proposed "green" $Ag-Mg(OH)_2$ nanocomposite becomes an ambitious candidate to remove various microbes and organic dyes from water sources. This represents a significant advance in the field of biosynthesized nanocomposites, and by harnessing the power of natural extracts from fruits like avocado peel, researchers can develop more innovative materials with tailored properties for a broader range of applications.

2. Experimental setup

2.1. Synthesis of avocado peel extract

Avocados were purchased from local markets and peeled. The avocado peel was washed with DI water to remove the flesh completely, then dried at 60°C for 24 hours and finely ground to reduce moisture for better preservation. The dry powder was then extracted through dispersion in DI water and magnetic stirring at 60°C for 1 hour [31]. The resulting suspension was finally vacuum filtered to obtain the avocado peel extract.

2.2. Synthesis of MgO via sol–gel method

50 mL of avocado peel extract was mixed with 250 mL of 0.2 $MMg\left(NO_3\right)_2$ solution, then 245 mL of 0.4 M NaOH solution was gradually added to the resulting mixture under magnetic stirring [32, 33]. The precipitate was washed by ethanol and vacuum filtered, then dried at 60°C for 12 hours. The dry solid was finally calcined at 550°C for 3 hours, producing the white MgO powder.

2.3. Synthesis of Ag-$Mg(OH)_2$ nanocomposite

The as-prepared MgO powder was added to a 0.001 M $AgNO_3$ solution and stirred for 10 minutes [7]. The avocado peel extract was gradually introduced into the resulting mixture and magnetically stirred for 30 minutes. The suspension was centrifuged and washed with ethanol to collect the solid, which was then dried at 60°C for 6 hours to yield a yellowish brown powder (i.e. the $Ag - Mg(OH)_2$ nanocomposite).

2.4. Adsorption of methylene blue in dark conditions

For this experiment, m gram of $Ag - Mg(OH)_2$ nanocomposite was added into V mL of C ppm methylene blue (MB) solution. The resulting mixture was vigorously stirred without light exposure to investigate the adsorption capacity of the material. After fixed time intervals, a portion of the sample suspension was collected and filtered to remove the solid. The UV-Vis technique was then used to determine the remaining concentration of MB, allowing one to calculate the adsorption capacity of $Ag - Mg(OH)_2$ and establish a specific isothermal adsorption model.

2.5. Catalytic activity of Ag-$Mg(OH)_2$ nanocomposite on the photodegradation of methylene blue

For this experiment, m gram of $Ag - Mg(OH)_2$ nanocomposite was added into V mL of C ppm MB solution. The resulting mixture was vigorously stirred and continuously illuminated at 45°C by a 30 W LED lamp (3000 lm, CCT $6000 - 6500$ K) to investigate the photocatalytic activity of the material. After fixed time intervals, a portion of the sample was collected and filtered to remove the solid. The UV-Vis technique was then used to determine the post-reaction concentration of MB , allowing one to calculate the removal efficiency, establish a reaction kinetic model and study the factors affecting the photodegradation of MB . Apart from reactions with various amounts of $Ag - Mg(OH)_2$, a blank run ($m = 0$) was also conducted; its yield was taken as a reference to accurately assess the photocatalytic activity of the nanocomposite.

2.6. Catalyst regeneration

After the photodegradation of MB , the spent $Ag - Mg(OH)_2$ nanocomposite was regenerated via chemical washes with 96° ethanol solvent. This step was to remove unreacted MB adsorbates. The washed solid was then vacuum filtered and dried at 80°C for 2 hours to obtain the regenerated $Ag - Mg(OH)_2$ nanocomposite, which was reused for additional reactions.

3. Results and discussion

3.1. UV–Vis spectroscopy

Fig. 1(a) shows a maximum absorption peak fluctuating within the wavelength range of 275−280 nm. This maximum absorption peak can be attributed to compounds belonging to the flavonoid group, specifically derivatives of quercetin: quercetin–diglucoside, quercetin−3−oarabinosyl–glucoside and rutin, which are three of the seven main polar organic compounds found in avocado peel according to the report by López-Cobo et al. when using HPLC-MS to analyze the composition of avocado peel [34, 35].

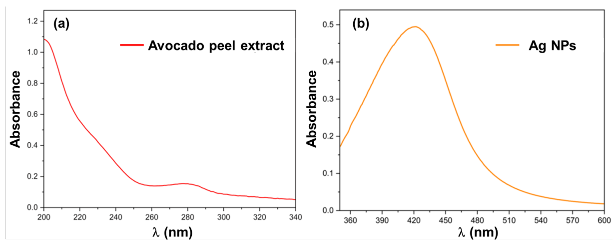

(a) (b)

Fig. 1. (a) UV–Vis absorption spectra of *Persea americana* peel extract and (b) silver nanoparticles synthesized from this extract.

Following the avocado peel extract-assisted synthesis of $Ag - Mg(OH)_2$ nanocomposites, Fig. 1(b) displays a maximum absorption peak at the wavelength of 422 nm , which is evident from the presence of Ag nanoparticles in the as-prepared sample. According to numerous studies, the maximum absorption peak of Ag nanoparticles typically fluctuates within the wavelength range of 420−460 nm due to the phenomenon of surface plasmon resonance, an important optical property of these nanoparticles [36, 37]. As referred to relevant works from which surface plasmon resonance peaks were used to evaluate nanoparticle sizes [38–40], the 422−nm wavelength associates with a spherical shape and a diameter of 25−35 nm for our biosynthesized Ag nanoparticles.

3.2. X–ray diffraction (XRD)

Fig. 2 shows the maximum diffraction peaks at 18.71° (001), 32.96° (100), 38.11° (011), 51.04° (102), 58.83° (110), 62.33° (111), 68.35° (103), and 72.16° (201), all of which are typical for $Mg(OH)_2$ (in agreement with AMCSD data 0014731 [41]). The presence of characteristic diffraction peaks of Ag, however, is not noticed. This can be explained by the small content of Ag in the sample and the Ag nanoparticles can be evenly dispersed on the surface.

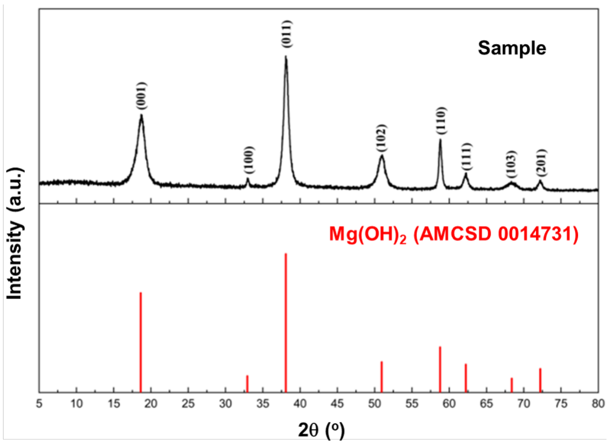

Fig. 2. XRD patterns of $Ag - Mg(OH)_2$ nanocomposite synthesized using *Persea americana* peel extract.

3.3. Scanning electron microscope (SEM)

From Fig. 3, it can be seen that MgO particles tend to agglomerate, which may be due to the high temperature heating process at 550°C. SEM images at magnifications of 150 k and 120 k, however, show that MgO particles reach nano-size with a size of about 50 nm .

SEM images from Fig. 4 show a relatively uniform distribution of small particles, whose sizes range from 20 nm to 50 nm , on the surface of the then-hydrated $Mg(OH)_2$ substrate. Combined with the energy dispersive X-ray spectrum (EDX), these finely distributed small particles are potentially Ag nanospheres, consistent with the morphology and size estimation from earlier discussed UV-Vis data.

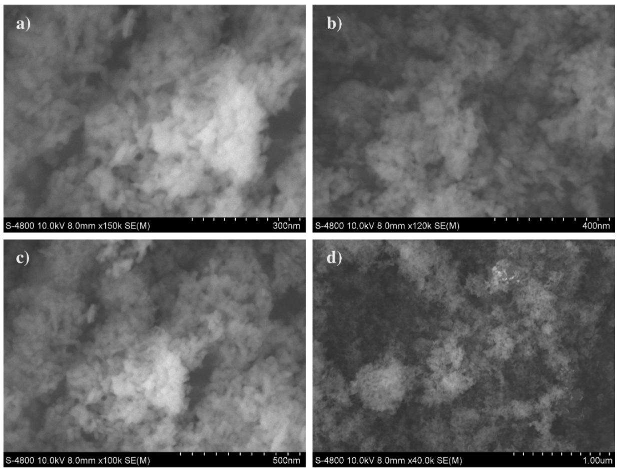

Fig. 3. SEM images of MgO prepared via the sol–gel method at magnifications of (a) 150k, (b) 120k, (c) 100k and (d) 40k.

At the same time, SEM images also show the presence of nanorods with diameters from 20− 50 nm and lengths of 250 − 300 nm. From Fig. 2, it can be seen that these nanorods are highly likely to be nanorods of $Mg(OH)_2$. The observed nanorod morphology is similar to that of $Mg(OH)_2$ nanorods reported in the study of Shah et al. [42].

3.4. Energy dispersive X–ray spectroscopy (EDX)

Fig. 4 shows that on the surface of the solid sample, there are three elements Ag, Mg, O. Mostly the presence of Mg and O, Ag accounts for low concentrations since the synthesis process uses low concentrations of $AgNO_3$. Besides, the ratio of O and Mg atoms is approximately equal to 2 , showing that the sample contains $Mg(OH)_2$.

3.5. Adsorption capacity of Ag-$Mg(OH)_2$ nanocomposite in the absence of light

From Fig. 5, it can be seen that the adsorption process of MB dye on the material at a concentration of 50 ppm increases rapidly in the first 30 minutes, then begins to slow down and reaches equilibrium after about 60 minutes. At smaller concentrations (10 ppm and 20 ppm), the adsorption process takes place faster and quickly reaches equilibrium after about 15 minutes. Such behavior can be ascribed to the initially large number of active centers on the surface of $Ag - Mg(OH)_2$ nanocomposite. As time elapses, these centers are substantially occupied by dye molecules, causing the number of centers on the surface of the material to decrease gradually, so the adsorption process will decelerate

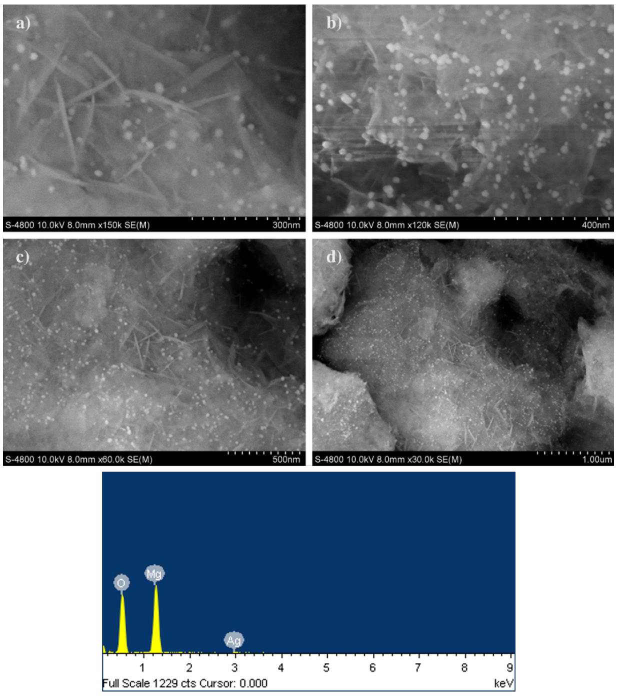

Fig. 4. SEM images of $Ag - Mg(OH)_2$ nanocomposite synthesized using *Persea americana* peel extract at magnifications of (a) 150k, (b) 120k, (c) 100k and (d) 40k; along with EDX spectrum of the material.

and reach equilibrium.

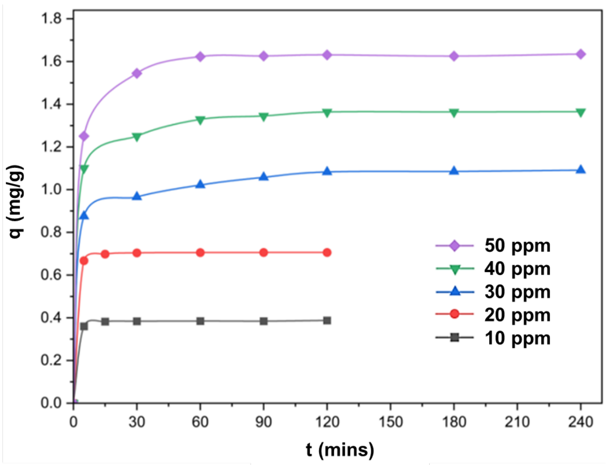

Fig. 5. Adsorption capacity of $Ag - Mg(OH)_2$ nanocomposite under dark conditions at different methylene blue concentrations over time ($d = 8\,g/L, T = 30°C$).

For each initial MB concentration, the equilibrium concentration and equilibrium adsorption capacity can be determined. These parameters are inferred from the slopes and y -intercepts of reciprocal and natural logarithm functions to test the respective compatibilities of Langmuir and Freundlich isothermal adsorption models (Fig. 6).

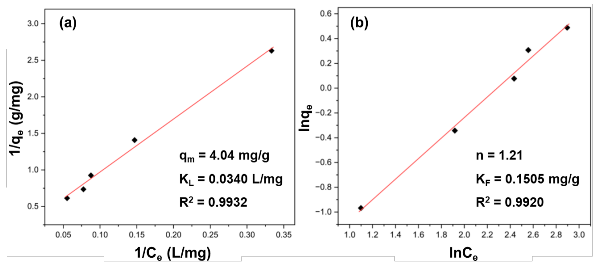

(a) (b)

Fig. 6. (a) Langmuir and (b) Freundlich adsorption isotherms of methylene blue on $Ag - Mg(OH)_2$ nanocomposite ($d = 8\,g/L, T = 30°C$).

It can be seen that both models give high R^2 coefficients (R^2 is 0.9932 for Langmuir and 0.9920 for Freundlich). In the Langmuir isotherm adsorption model, the K_L constant is 0.034 L/ mg and the maximum MB adsorption capacity of the material is 4.04 mg/g.

Meanwhile, in the Freundlich isothermal adsorption model, the K_F constant is 0.1505 mg/g and the coefficient n is 1.21 . From the above analysis, it can be concluded that the experimental isothermal adsorption data of MB on the material are compatible with both Langmuir and Freundlich isotherm models. Such findings technically indicate rather simple adsorption mechanisms of MB molecules on $Ag - Mg(OH)_2$, compared to more complex interactions between thionine dye molecules (TH) and magnetic chitosan-clay/benzoin/ Fe_3O_4 adsorbents - including electrostatic attractions, $n - \pi$ interaction, hydrogen bonding and Yoshida H− bonding [43]. Assuming an average cross-sectional area of $130Å^2$ for each MB molecule ($MW = 319.85\,g/mol$) [44], the maximum adsorption capacity from the Langmuir isotherm results in a surface area of $9.88\,m^2/g$ for $Ag - Mg(OH)_2$.

3.6. Kinetic model of photocatalytic reaction

The change of MB concentration over time at two initial concentrations of 10 ppm and 20 ppm was investigated and results were obtained as shown in Fig. 7(a).

The photodegradation of aqueous MB on $Ag - Mg(OH)_2$ nanocomposite proceeds through three essential steps [21, 45]. At first, finely dispersed Ag nanospheres significantly enhance UV light-induced electron-hole separation in the $Mg(OH)_2$ semiconductor. Due to the exceptional electrical conductivity, these anchored Ag nanoparticles exhibit surface plasmon resonance to improve visible

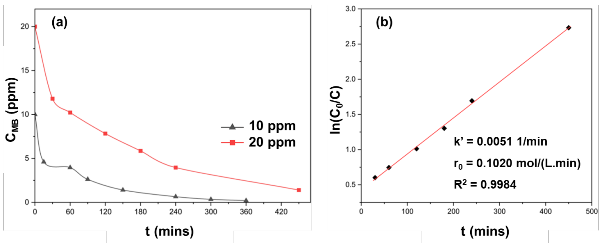

(a) (b)

Fig. 7. (a) Evolution of methylene blue content in aqueous solution with initial concentrations of 10 ppm and 20 ppm under UV irradiation ($d = 8\,g/L, T = 45°C$). and (b) pseudo first−order kinetic model at 20 ppm methylene blue concentration.

light absorption and function as photoelectron traps, suppressing the recombination rate of electron-hole pairs to supply sufficient charge carriers for sequential reactions. Reactive oxygen species (ROS) are then generated from interactions between separated charge carriers and components in the aqueous solution. In particular, excited electrons in the conduction band of $Mg(OH)_2$ (or those trapped by Ag nanoparticles) react with dissolved oxygen molecules to produce $O_2\bullet^-$radicals, while the holes in the valence band target water molecules or OH^-anions to yield •OH radicals. Finally, the nascent ROS species attack methylene blue adsorbates to oxidize and decolorize the dye, converting its molecules into simpler, non-toxic components. The overall mechanism can be summarized as follows:

(i) $\mathbf{MB}_{aq} + Ag{-}Mg(OH)_{2\ s} \leftrightarrow \mathbf{MB} - Ag - Mg(OH)_{2\ ads}$

(ii) $Ag{-}Mg(OH)_{2\ ads}$ $+h\nu \leftrightarrow Ag{-}Mg(OH)_2(e^-_{cb},\ h^+{}_{vb})_{ads}$

(iii) $Ag{-}Mg(OH)_2\ (e^-_{cb})_{ads}$ $+O_{2\ aq} \rightarrow Ag{-}Mg(OH)_2(O_2\bullet^-)_{ads}$

(iv) $Ag{-}Mg(OH)_2\ (h^+{}_{vb})_{ads}$ $+H_2O \rightarrow Ag{-}Mg(OH)_2(\bullet OH)_{ads} + H^+{}_{aq}$

(v) $Ag{-}Mg(OH)_2\ (\ h^+{}_{vb})_{ads}$ $+OH^-_{aq} \rightarrow Ag{-}Mg(OH)_2(\bullet OH)_{ads}$

(vi) $Ag{-}Mg(OH)_2\ (O_2\bullet^-)_{ads}$ $+$ $\mathbf{MB}{-}Ag{-}Mg(OH)_{2\ ads} \rightarrow$ degradation products

(vii) $Ag{-}Mg(OH)_2(\bullet OH)_{ads}$ $+\mathbf{MB}{-}Ag{-}Mg(OH)_2(\bullet OH)_{ads} \rightarrow$ degradation products

The Langmuir-Hinshelwood model is often used to describe such photodegradation kinetics, provided that intermediate and post-decomposition products do not adsorb competitively on the catalyst surface. At low initial MB concentrations, the photocatalytic reaction rate is considered first-order, and the apparent kinetic equation is expressed through a linearized natural logarithm function:

$$\ln\left(\frac{C_o}{C}\right) = k' \cdot t \tag{1}$$

In which, C(ppm) is the MB concentration at time t, C_o is the initial MB concentration and k' is the apparent first-order reaction rate constant (min^{-1}).

To assess the compatibility with the as-described kinetic model, the linear regression method is used to construct a graph of $\ln(C_o/C)$ versus time (Fig. 7(b)), and the slope of the line allows to determine the reaction rate constant k'.

From Fig. 7(b), it can be seen that at $C_{0MB} = 20ppm, R^2$ is relatively high (0.9984), thus the MB photodegradation reaction follows the Langmuir-Hinshelwood first-order kinetic model, with the rate constant value of $k' = 0.0051\ min^{-1}$ at the reaction temperature of 45°C. Such finding is comparable to Hasan et al.'s work [29], where photodegradation reactions of MB and TB on $Ag@Fe_3O_4$ nanocomposites both satisfy first-order kinetics.

3.7. Effect of methylene blue concentration on photocatalytic reaction performance

The initial concentration of organic pigments in wastewater is one of the important factors affecting the performance of the photodegradation process of dyes. While the MB adsorption process under dark conditions only removes a certain amount of MB and reaches equilibrium after 60 minutes (Fig. 5), the MB treatment efficiency increases following UV irradiation (Fig. 8), indicating that photodegradation occurs and MB molecules are eventually decomposed.

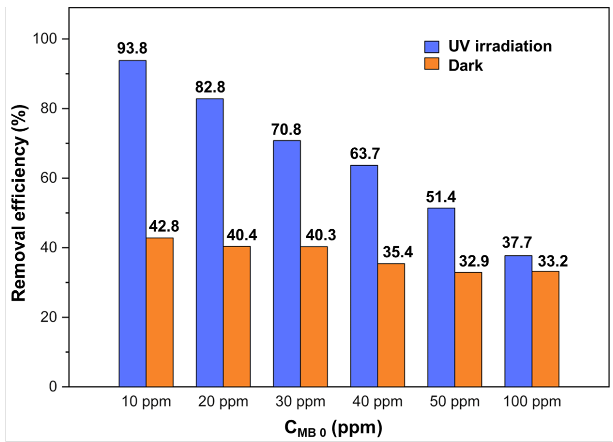

Fig. 8. The influence of methylene blue initial concentration on photocatalytic reaction performance ($d = 8\,g/L,\ T = 45°C,\ t = 180$ mins).

Fig. 8 also shows that the MB treatment efficiency under UV irradiation decreases from 93.8% to 37.7% when increasing the initial MB concentration from 10 ppm to 100 ppm , and the gradual adsorption process plays a major role in the MB treatment process at high concentrations (at 100 ppm , the MB treatment efficiencies with and without illumination are mostly identical). This can be explained by the formation of $OH^{\cdot}$ radicals on the surface of the catalyst and the reactivity between $OH^{\bullet}$ radicals and dyes [46–49]. An increase in the initial concentration of MB leads to a larger amount of MB molecules anchored on active sites of the catalyst, partially blocking the adsorption of hydroxyl anions (OH^-) on these sites, thus dropping the rate of formation of $OH^{\cdot}$ radicals. At the same time, according to the Beer-Lambert law, high concentrations of MB render the path in solution through which light photons travel more tortuous, thus reducing the number of photons to access the catalytic surface of $Ag - Mg(OH)_2$. In other words, the nanocomposite catalyst will absorb much less photons, resulting in a significant decrease in the efficiency of photodegradation. From Fig. 8, the initial MB concentration of 20 ppm leads to a significantly high degradation efficiency of 82.8% after 3 hours of photocatalytic reaction, therefore this concentration is selected for catalytic optimization. The observed experimental results also render avocado peel extract-Ag- $Mg(OH)_2$ nanocomposites a good option compared to some other photocatalysts in similar MB degrading conditions (Table 1).

3.8. Effect of the ratio between catalyst mass and solution volume on photocatalytic reaction performance

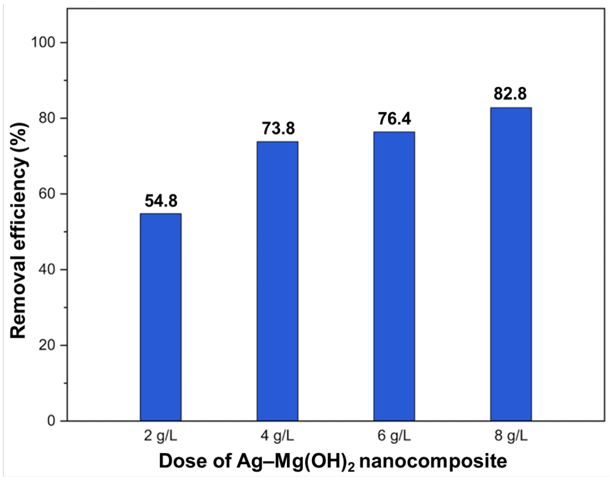

Fig. 9. The influence of the dose of $Ag-Mg(OH)_2$ nanocomposite on the photodegradation efficiency of MB under UV irradiation ($C_{MB0} = 20ppm, T = 45°C, t = 180mins$).

Investigating the influence of catalyst mass on photodegradation efficiency is also an issue that needs to be considered in order to minimize costs from using materials while still ensuring high treatment efficiency.

Fig. 9 shows that the decomposition efficiency of MB increases as the volume of material increases, as the surface area of the material is larger, creating favorable conditions for MB adsorption and light absorption, thereby speeding up the reaction. At high material dosages, however, the turbidity of the solution also increases (due to additional light scattering of the material layer near the light source position), causing an obstructing effect, limiting the transmission of light into the solution. As a result, the photodegradation rate tends to increase slowly, up to a certain dosage limit where excess turbidity may reduce the MB removal efficiency [54]. Apparently, when the material dosage is doubled from 2 g/L to 4 g/L, such efficiency increases significantly (nearly 20%). Beyond this limit (from 4 g/L to 8 g/L), however, it does not increase much (less than 10%), causing a catalyst waste which is not economically beneficial.

To sum up, investigating the effect of $Ag-Mg(OH)_2$ dosage on MB photodegradation essentially helps reduce material costs while maintaining remarkable catalytic performances. It is therefore necessary to properly balance between photodegradation activities and economic efficiency, as well as alleviating the undesirable silver ion release to the environment. In this study, the ratio between material mass and MB solution volume of 4 g/L is considered optimal in terms of catalytic behavior and saving costs.

3.9. Regeneration of post-reaction Ag-$Mg(OH)_2$ nanocomposite

Investigating the ability to regenerate materials is essential to optimize resource use, save costs while ensuring performance and stable operation.

Fig. 10 demonstrates that following two regeneration cycles, although the spent $Ag-Mg(OH)_2$ mostly retains catalytic activity in photodegradation, the 3-hour treatment efficiency has decreased by approximately 20% with respect to that of the original material.

This could be ascribed to the loss of Ag nanoparticles following washes with ethanol, or more possibly, the incomplete removal of a fraction of adsorbed MB and decomposition products from the surface of the catalytic material, which presumably limits the ability of MB to access active centers during the next use. To alleviate metal leaching, a less polar solvent (e.g. acetone) may work for the washing step, while steric hindrance could be reduced by an increased drying temperature up to $110-120°C$, which technically initiates the decomposition of methylene blue, but not sufficiently high to trigger the sintering of Ag nanoparticles.

In other words, since the main application of $Ag-Mg(OH)_2$ nanocomposites is catalyzing the photodegradation of organic dyes, it is essential to control the risk of releasing Ag^+ions or Ag nanoparticles into the aqueous medium. As referred from Jiang et al.'s work [55], such release can be mitigated by three governing factors: (1) strong bonds between phenolic ligands and surface Ag nanoparticles, (2) medium or long carbon chain in ligands to obstruct the leaching path, and (3) high Ag^+ion attraction to surface-bound ligands or the $Mg(OH)_2$ support for potential readsorption. As mentioned in section 3.1, the main phenolic compounds from avocado peel extract are quercetin and its derivatives, all of which are bulky molecules acting as both reducing and capping agents and generally forming strong bonds with Ag nanoparticles.

The loss of these ligands in the as-prepared material may partially result in Ag^+ion release; nevertheless, the support of $Mg(OH)_2$ nanorods may effectively capture both free Ag nanoparticles and Ag^+ions to minimize environmental toxicity [56].

4. Conclusions

In this study, $Ag-Mg(OH)_2$ nanocomposites were successfully synthesized through the use of avocado peel extract to reduce the precursor $AgNO_3$ from its 0.001 M aqueous solution. Combined characterization results from UV-Vis, XRD, SEM and EDX confirm the presence of uniformly dispersed Ag nanoparticles (20-50 nm in diameter) on the surface of $Mg(OH)_2$ nanorods ($250-300$ nm in length). The catalytic activity of the biosynthesized nanomaterial was investigated through the photodegradation of methylene blue (MB) solutions, revealing a remarkable decomposition efficiency of 82.8% at 45°C after 3 hours from an initial MB concentration of 20 ppm and a nanomaterial mass - liquid volume ratio of 8 g/L. Studies on factors affecting the nanocomposites' catalytic performance also provide valuable data. The chemisorption process without UV illumination is compatible with both Langmuir ($K_L = 0.034$ L/mg) and Freundlich ($K_F = 0.1505$mg/g) isotherms, while the subsequent photodegradation of MB follows pseudo first-order kinetics ($k' = 0.0051\ min^{-1}$), and the decomposition efficiency gradually decreases with increasing initial concentrations of MB. Regarding catalyst loading, the nanomaterial mass - liquid volume ratio of

Table 1. Equivalent methylene blue degradation efficiencies of some nanophotocatalysts under UV irradiation ($C_{MB0} = 20ppm,\ T = 30 - 45°C,\ t = 180mins$).

Nanophotocatalyst	Degradation efficiency (%)	Reference
$CeO_2@Sp$	88.8	[50]
$Ag - Mg(OH)_2$	82.8	This work
$Ag - CuO$	80.0	[51]
TiO_2/Nd_2O_3	72.9	[52]
TiO_2	62.7	[52]
$ZnO/clay$	58.0	[53]

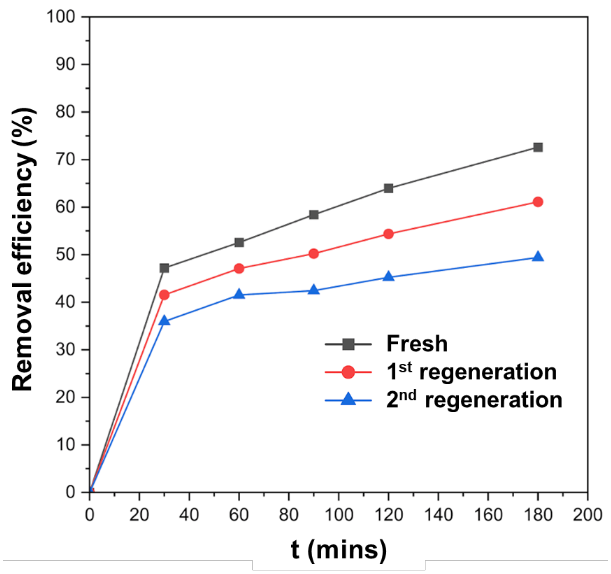

Fig. 10. Catalytic activity of $Ag - Mg(OH)_2$ nanocomposite after 2 regeneration cycles under UV irradiation ($d = 4\ g/L,\ T = 45°C,\ C_{MB0} = 20ppm$).

4 g/L is technically more efficient than 8 g/L in terms of both catalytic performance and economical aspects. In addition, the spent $Ag - Mg(OH)_2$ nanocomposite can be regenerated through simple washes with ethanol and hours of drying before reused, exhibiting a comparable MB conversion with respect to the fresh catalyst's performance. In general, this research paves way for future studies to further optimize the biosynthesis of $Ag - Mg(OH)_2$ nanocomposites, in terms of both greener methods and material composition, and to exploit their uses in the photodegradation of other common industrial organic dyes, effectively contributing to the field of wastewater remediation.

Acknowledgements

This research is funded by Vietnam National University Ho Chi Minh City (VNU-HCM) under grant number: C2023-20-11.

References

[1] V. K. Sharma, R. A. Yngard, and Y. Lin, (2009) *"Silver nanoparticles: green synthesis and their antimicrobial activities"* **Advances in colloid and interface science** ***145***(1-2): 83–96. DOI: 10.1016/j.cis.2008.09.002.

[2] O. Fruhwirth, G. Herzog, I. Hollerer, and A. Rachetti, (1985) *"Dissolution and hydration kinetics of MgO"* **Surface Technology** ***24***(3): 301–317. DOI: 10.1016/0376-4583(85)90080-9.

[3] S. W. Kim, I. Kim, and D. J. Moon, (2013) *"Synthesis and characterization of magnesium oxide supported catalysts with a meso-macropore structure"* **Journal of nanoscience and nanotechnology** ***13***(8): 5750–5753. DOI: 10.1166/jnn.2013.7038.

[4] N. M. Julkapli and S. Bagheri, (2016) *"Magnesium oxide as a heterogeneous catalyst support"* **Reviews in Inorganic Chemistry** ***36***(1): 1–41. DOI: 10.1515/revic-2015-0010.

[5] D. Jin, X. Gu, X. Yu, G. Ding, H. Zhu, and K. Yao, (2008) *"Hydrothermal synthesis and characterization of hexagonal $Mg(OH)_2$ nano-flake as a flame retardant"* **Materials Chemistry and Physics** ***112***(3): 962–965. DOI: 10.1016/j.matchemphys.2008.07.058.

[6] A. A. Pilarska, Ł. Klapiszewski, and T. Jesionowski, (2017) *"Recent development in the synthesis, modification and application of $Mg(OH)_2$ and MgO: A review"* **Powder Technology** ***319***: 373–407. DOI: 10.1016/j.powtec.2017.07.009.

[7] M. Jayapriya, K. Premkumar, M. Arulmozhi, and K. Karthikeyan, (2020) *"One-step biological synthesis of cauliflower-like Ag/MgO nanocomposite with antibacterial, anticancer, and catalytic activity towards anthropogenic pollutants"* **Research on Chemical Intermediates** ***46***(3): 1771–1788. DOI: 10.1007/s11164-019-04062-1.

[8] M. Rajkumar, S. D. Presley, F. Menaa, S. E. I. Elbehairi, M. Y. Alfaifi, A. A. Shati, A. E. Albalawi, N. A. Althobaiti, D. Kirubakaran, P. Govindaraj, et al., (2024) *"Biosynthesis and biological activities of magnesium hydroxide nanoparticles using Tinospora cordifolia leaf extract"* **Bioprocess and Biosystems Engineering** ***47***: 2111–2129. DOI: 10.1007/s00449-024-03089-y.

[9] B. Gherbi, S. E. Laouini, S. Meneceur, A. Bouafia, H. Hemmami, M. L. Tedjani, G. Thiripuranathar, A. Barhoum, and F. Menaa, (2022) *"Effect of pH value on the bandgap energy and particles size for biosynthesis of ZnO nanoparticles: Efficiency for photocatalytic adsorption of methyl orange"* **Sustainability** ***14***(18): 11300. DOI: 10.3390/su141811300.

[10] K. Alia, D. Atia, M. L. Tedjani, G. G. Hasan, H. A. Mohammed, S. E. Laouini, M. M. Abdullah, and F. Menaa, (2024) *"Characterization optimization of synthesis Chitosanclay/benzoin/Fe_3O_4 composite for adsorption of Thionine dye by design expert study"* **Scientific Reports** ***14***(1): 23373. DOI: 10.1038/s41598-024-75016-w.

[11] I. Trujillo-Mayol, C. Céspedes-Acuña, F. L. Silva, and J. Alarcón-Enos, (2019) *"Improvement of the polyphenol extraction from avocado peel by assisted ultrasound and microwaves"* **Journal of Food Process Engineering** ***42***(6): e13197. DOI: 10.1111/jfpe.13197.

[12] D. A. Kumar, V. Palanichamy, and S. M. Roopan, (2014) *"Green synthesis of silver nanoparticles using Alternanthera dentata leaf extract at room temperature and their antimicrobial activity"* **Spectrochimica Acta Part A: Molecular and Biomolecular Spectroscopy** ***127***: 168–171. DOI: 10.1016/j.saa.2014.02.058.

[13] R. Colombo and A. Papetti, (2019) *"Avocado (Persea americana Mill.) by-products and their impact: From bioactive compounds to biomass energy and sorbent material for removing contaminants. A review"* **International Journal of Food Science and Technology** ***54***(4): 943–951. DOI: 10.1111/ijfs.14143.

[14] M. Dahmardnezhad, S. H. Rafsanjani, S. Sabbaghi, N. Baghinia, N. Fooladivanda, E. Peyravi, M.-R. Baghinia, Y. Parsa, H. G. Kolagar, F. Saremi, et al., (2024) *"A Novel Persian Herbal Syrups: Preventive and Curative Effects of Syrup Formulation of Achillea. millefolium L. against Ethylene Glycol Induced Urolithiasis in Rats: Novel Persian Herbal Syrups and Urolithiasis"* **Galen Medical Journal** ***13***: e3317–e3317. DOI: 10.31661/gmj.v13i.3317.

[15] M. Abdolahad, M. Janmaleki, S. Mohajerzadeh, O. Akhavan, and S. Abbasi, (2013) *"Polyphenols attached graphene nanosheets for high efficiency NIR mediated photodestruction of cancer cells"* **Materials Science and Engineering: C** ***33***(3): 1498–1505. DOI: 10.1016/j.msec.2012.12.052.

[16] G. R. Velderrain-Rodriguez, J. Quero, J. Osada, O. Martin-Belloso, and M. J. Rodríguez-Yoldi, (2021) *"Phenolic-rich extracts from avocado fruit residues as functional food ingredients with antioxidant and antiproliferative properties"* **Biomolecules** ***11***(7): 977. DOI: 10.3390/biom11070977.

[17] F. Özbaş, (2024) *"Sustainable synthesis of green Cu_2O nanoparticles using avocado peel extract as biowaste source"* **Journal of the Turkish Chemical Society Section A: Chemistry** ***11***(1): 303–312. DOI: 10.18596/jotcsa.1391735.

[18] O. Akhavan and E. Ghaderi, (2010) *"Self-accumulated Ag nanoparticles on mesoporous TiO_2 thin film with high bactericidal activities"* **Surface and Coatings Technology** ***204***(21-22): 3676–3683. DOI: 10.1016/j.surfcoat.2010.04.048.

[19] M. A Bhosale and B. M Bhanage, (2015) *"Silver nanoparticles: Synthesis, characterization and their application as a sustainable catalyst for organic transformations"* **Current Organic Chemistry** ***19***(8): 708–727. DOI: 10.2174/1385272819666150207001154.

[20] M. Ramezani Farani, M. Farsadrooh, I. Zare, A. Gholami, and O. Akhavan, (2023) *"Green synthesis of magnesium oxide nanoparticles and nanocomposites for photocatalytic antimicrobial, antibiofilm and antifungal applications"* **Catalysts** ***13***(4): 642. DOI: 10.3390/catal13040642.

[21] B. Uzair, A. Liaqat, H. Iqbal, B. Menaa, A. Razzaq, G. Thiripuranathar, N. Fatima Rana, and F. Menaa, (2020) *"Green and cost-effective synthesis of metallic nanoparticles by algae: Safe methods for translational medicine"* **Bioengineering** ***7***(4): 129. DOI: 10.3390/bioengineering7040129.

[22] J. Zhou, Y. Yang, and Z. Li, (2024) *"Efficient and fast arsenate removal from water by in-situ formed magnesium hydroxide"* **Scientific Reports** ***14***(1): 21232. DOI: 10.1038/s41598-024-72258-6.

[23] N. A. Amro, L. P. Kotra, K. Wadu-Mesthrige, A. Bulychev, S. Mobashery, and G.-y. Liu, (2000) *"High-resolution atomic force microscopy studies of the Escherichia coli outer membrane: structural basis for permeability"* **Langmuir** ***16***(6): 2789–2796. DOI: 10.1021/la991013x.

[24] Y. Zidane, S. E. Laouini, A. Bouafia, S. Meneceur, M. L. Tedjani, S. A. Alshareef, H. A. Almukhlifi, K. Al-Essa, E. M. Al-Essa, M. M. Rahman, et al., (2022) *"Green synthesis of multifunctional MgO@ AgO/Ag_2O nanocomposite for photocatalytic degradation of methylene blue and toluidine blue"* **Frontiers in Chemistry** ***10***: 1083596. DOI: 10.3389/fchem.2022.1083596.

[25] I. Khan, K. Saeed, I. Zekker, B. Zhang, A. H. Hendi, A. Ahmad, S. Ahmad, N. Zada, H. Ahmad, L. A. Shah, et al., (2022) *"Review on methylene blue: its properties, uses, toxicity and photodegradation"* **Water** ***14***(2): 242. DOI: 10.3390/w14020242.

[26] A. L. Linsebigler, G. Lu, and J. T. Yates Jr, (1995) *"Photocatalysis on TiO_2 surfaces: principles, mechanisms, and selected results"* **Chemical reviews** ***95***(3): 735–758. DOI: 10.1021/cr00035a013.

[27] M. Matalkeh, G. K. Nasrallah, F. M. Shurrab, E. S. Al-Absi, W. Mohammed, A. Elzatahry, and K. M. Saoud, (2022) *"Visible light photocatalytic activity of Ag/WO_3 nanoparticles and its antibacterial activity under ambient light and in the dark"* **Results in Engineering** ***13***: 100313. DOI: 10.1016/j.rineng.2021.100313.

[28] Z. Qiu, B. Wang, X. Zhou, S. Yang, Q. Gao, X. Cai, S. Zhang, and Y. Fang, (2022) *"CdS@ $Mg(OH)_2$ core/shell composite photocatalyst for efficient visible-light photocatalytic overall water splitting"* **International Journal of Hydrogen Energy** ***47***(14): 8729–8738. DOI: 10.1016/j.ijhydene.2021.12.216.

[29] G. G. Hasan, S. E. Laouini, A. Khelef, H. A. Mohammed, M. Althamthami, S. Meneceur, F. Alharthi, S. A. Alshareef, and F. Menaa, (2024) *"Efficient treatment of oily wastewater, antibacterial activity, and photodegradation of organic dyes using biosynthesized Ag@ Fe_3O_4 nanocomposite"* **Bioprocess and Biosystems Engineering** ***47***(1): 75–90. DOI: 10.1007/s00449-023-02946-6.

[30] F. A. Alharthi, A. A. Alghamdi, N. Al-Zaqri, H. S. Alanazi, A. A. Alsyahi, A. E. Marghany, and N. Ahmad, (2020) *"Facile one-pot green synthesis of Ag–ZnO Nanocomposites using potato peeland their Ag concentration dependent photocatalytic properties"* **Scientific Reports** ***10***(1): 20229. DOI: 10.1038/s41598-020-77426-y.

[31] K. Murugesan, K. Tareke, M. Gezehegn, M. Kebede, A. Yazie, and G. Diyana, (2019) *"Rapid development of activated carbon and ZnO nanoparticles via green waste conversion using avocado fruit peel powder and its high performance efficiency in aqueous dye removal application"* **Journal of Inorganic and Organometallic Polymers and Materials** ***29***(4): 1368–1374. DOI: 10.1007/s10904-019-01101-7.

[32] B. L. Cushing, V. L. Kolesnichenko, and C. J. O'connor, (2004) *"Recent advances in the liquid-phase syntheses of inorganic nanoparticles"* **Chemical reviews** ***104***(9): 3893–3946. DOI: 10.1021/cr030027b.

[33] N. Khanna and A. R. Kumar, (2018) *"Preparation and characterization of MgO nanoparticles by sol–gel method"* **Advanced Science Letters** ***24***(8): 5708–5711. DOI: 10.1166/asl.2018.12182.

[34] B. Kumar and L. Cumbal, (2016) *"UV-Vis, FTIR and antioxidant study of Persea americana (Avocado) leaf and fruit: a comparison"*: URL: https://dspace.ucuenca.edu.ec/500.

[35] A. López-Cobo, A. M. Gómez-Caravaca, F. Pasini, M. F. Caboni, A. Segura-Carretero, and A. Fernández-Gutiérrez, (2016) *"HPLC-DAD-ESI-QTOF-MS and HPLC-FLD-MS as valuable tools for the determination of phenolic and other polar compounds in the edible part and by-products of avocado"* **Lwt** ***73***: 505–513. DOI: 10.1016/j.lwt.2016.06.049.

[36] R. Das, S. S. Nath, D. Chakdar, G. Gope, and R. Bhattacharjee, (2010) *"Synthesis of silver nanoparticles and their optical properties"* **Journal of Experimental Nanoscience** ***5***(4): 357–362. DOI: 10.1080/17458080903583915.

[37] L. Mahmudin, E. Suharyadi, A. B. S. Utomo, and K. Abraha, (2015) *"Optical properties of silver nanoparticles for surface plasmon resonance (SPR)-based biosensor applications"* **Journal of Modern Physics** ***6***(8): 1071–1076. DOI: 10.4236/jmp.2015.68111.

[38] A. Babapour, O. Akhavan, R. Azimirad, and A. Moshfegh, (2006) *"Physical characteristics of heat-treated nano-silvers dispersed in sol–gel silica matrix"* **Nanotechnology** ***17***(3): 763–771. DOI: 10.1088/0957-4484/17/3/025.

[39] A. Naghizadeh, Z. M. Mizwari, S. M. Ghoreishi, S. Lashgari, S. Mortazavi-Derazkola, and B. Rezaie, (2021) *"Biogenic and eco-benign synthesis of silver nanoparticles using jujube core extract and its performance in catalytic and pharmaceutical applications: Removal of industrial contaminants and in-vitro antibacterial and anticancer activities"* **Environmental Technology & Innovation** ***23***: 101560. DOI: 10.1016/j.eti.2021.101560.

[40] M. Ansari, S. Ahmed, A. Abbasi, M. T. Khan, M. Subhan, N. A. Bukhari, A. A. Hatamleh, and N. R. Abdelsalam, (2023) *"Plant mediated fabrication of silver nanoparticles, process optimization, and impact on tomato plant"* **Scientific Reports** ***13***(1): 18048. DOI: 10.1038/s41598-023-45038-x.

[41] R. T. Downs and M. Hall-Wallace, (2003) *"The American Mineralogist crystal structure database"* **American mineralogist** *88*(1): 247–250. URL: https://pubs.geoscienceworld.org/msa/ammin/article-pdf/88/1/247/3609817/31_1025downs.pdf.

[42] M. Shah and F. Al-Marzouki, (2011) *"A simple and safe method for preparation of $Mg(OH)_2$ nanorods in ambient air"* **International Journal of Nano Dimension** 2(2): 111–116. DOI: 10.7508/ijnd.2011.02.003.

[43] U. Wijesinghe, G. Thiripuranathar, H. Iqbal, and F. Menaa, (2021) *"Biomimetic synthesis, characterization, and evaluation of fluorescence resonance energy transfer, photoluminescence, and photocatalytic activity of zinc oxide nanoparticles"* **Sustainability** *13*(4): 2004. DOI: 10.3390/su13042004.

[44] B. B. Tewari and C. O. Thornton, (2010) *"Use of basic Methylene Blue Dye for specific surface area measurement of metal hexacyanoferrate (II) complexes"* **Revista de la Sociedad Química del Perú** *76*(4): 330–335.

[45] N. Ramesh, C. W. Lai, M. R. B. Johan, S. M. Mousavi, I. A. Badruddin, A. Kumar, G. Sharma, and F. Gapsari, (2024) *"Progress in photocatalytic degradation of industrial organic dye by utilising the silver doped titanium dioxide nanocomposite"* **Heliyon** *10*(24): DOI: 10.1016/j.heliyon.2024.e40998.

[46] R. Farouq, (2022) *"Coupling adsorption-photocatalytic degradation of methylene blue and maxilon red"* **Journal of Fluorescence** *32*(4): 1381–1388. DOI: 10.1007/s10895-022-02934-1.

[47] H. Hidaka, J. Zhao, E. Pelizzetti, and N. Serpone, (1992) *"Photodegradation of surfactants. 8. Comparison of photocatalytic processes between anionic DBS and cationic BDDAC on the titania surface"* **The Journal of Physical Chemistry** *96*(5): 2226–2230. DOI: 10.1021/j100184a037.

[48] N. M. Mahmoodi, J. Abdi, M. Oveisi, M. A. Asli, and M. Vossoughi, (2018) *"Metal-organic framework (MIL-100 (Fe)): Synthesis, detailed photocatalytic dye degradation ability in colored textile wastewater and recycling"* **Materials Research Bulletin** *100*: 357–366. DOI: 10.1016/j.materresbull.2017.12.033.

[49] J.-J. Du, Y.-P. Yuan, J.-X. Sun, F.-M. Peng, X. Jiang, L.-G. Qiu, A.-J. Xie, Y.-H. Shen, and J.-F. Zhu, (2011) *"New photocatalysts based on MIL-53 metal–organic frameworks for the decolorization of methylene blue dye"* **Journal of hazardous materials** *190*(1-3): 945–951. DOI: 10.1016/j.jhazmat.2011.04.029.

[50] M. H. Ali, M. S. Abdelkarim, and A. D. Al-Afify, (2024) *"Characterization and photodegradation of methylene blue dye using bio-synthesized cerium oxide nanoparticles with Spirulina platensis extract"* **Discover Applied Sciences** *6*(3): 94. DOI: 10.1007/s42452-024-05736-1.

[51] M. Farooq, S. Shujah, K. Tahir, S. T. Hussain, A. U. Khan, Z. M. Almarhoon, K. F. Alabbosh, A. A. Alanazi, T. M. Althagafi, and M. E. Zaki, (2024) *"Phytoassisted synthesis of CuO and Ag–CuO nanocomposite, characterization, chemical sensing of ammonia, degradation of methylene blue"* **Scientific Reports** *14*(1): 1618. DOI: 10.1038/s41598-024-51391-2.

[52] G. Liu, M. Mamat, Y. Baikeli, and X. Dong, (2024) *"Photocatalytic degradation of methylene blue by TiO_2/Nd_2O_3 composite thin films"* **Heliyon** *10*(9): DOI: 10.1016/j.heliyon.2024.e29894.

[53] S. Modi, V. K. Yadav, D. Ali, N. Choudhary, S. Alarifi, D. K. Sahoo, A. Patel, and M. H. Fulekar, (2023) *"Photocatalytic degradation of methylene blue from aqueous solutions by using nano-ZnO/kaolin-clay-based nanocomposite"* **Water** *15*(22): 3915. DOI: 10.3390/w15223915.

[54] J. Bandara, J. Kiwi, R. Humphry-Baker, and C. Pulgarin, (1996) *"Oxidative degradation and fluorescence of a non-biodegradable brightener via titania suspensions: implications for the natural cycle"* **Journal of Advanced Oxidation Technologies** *1*(2): 126–137. DOI: 10.1515/jaots-1996-0204.

[55] Y.-M. Long, L.-G. Hu, X.-T. Yan, X.-C. Zhao, Q.-F. Zhou, Y. Cai, and G.-B. Jiang, (2017) *"Surface ligand controls silver ion release of nanosilver and its antibacterial activity against Escherichia coli"* **International journal of nanomedicine**: 3193–3206. DOI: 10.2147/IJN.S132327.

[56] W. Yin, M. Liu, Y.-H. Wang, Y. Huang, T.-L. Zhao, Q.-Z. Yao, S.-Q. Fu, and G.-T. Zhou, (2022) *"$Fe_3O_4-Mg(OH)_2$ nanocomposite as a scavenger for silver nanoparticles: Rational design, facile synthesis, and enhanced performance"* **Environmental research** *212*: 113292. DOI: 10.1016/j.envres.2022.113292.